First-principles characterization of the anisotropy of theoretical strength and the stress–strain relation for a TiAl intermetallic compound

2009 J. Phys.: Condens. Matter 21 175407

(http://iopscience.iop.org/0953-8984/21/17/175407)

J. Phys.: Condens. Matter **21** (2009) 175407 (9pp) doi:10.1088/0953-8984/21/17/175407

First-principles characterization of the anisotropy of theoretical strength and the stress–strain relation for a TiAl intermetallic compound

Hong-Bo Zhou[1], **Ying Zhang**[1], **Yue-Lin Liu**[1], **Masanori Kohyama**[2], **Peng-Gang Yin**[3] **and Guang-Hong Lu**[1]

[1] School of Science, Beijing University of Aeronautics and Astronautics, Beijing 100191, People's Republic of China
[2] Research Institute of Ubiquitous Energy Devices, National Institute of Advanced Industrial Science and Technology, Osaka 563-8577, Japan
[3] School of Materials Science and Engineering, Beijing University of Aeronautics and Astronautics, Beijing 100191, People's Republic of China

E-mail: pgyin@buaa.edu.cn and LGH@buaa.edu.cn

Received 23 December 2008, in final form 23 February 2009
Published 30 March 2009
Online at stacks.iop.org/JPhysCM/21/175407

Abstract

We perform first-principles computational tensile and compressive tests (FPCTT and FPCCT) to investigate the intrinsic bonding and mechanical properties of a γ-TiAl intermetallic compound ($L1_0$ structure) using a first-principles total energy method. We found that the stress–strain relations and the corresponding theoretical tensile strengths exhibit strong anisotropy in the [001], [100] and [110] crystalline directions, originating from the structural anisotropy of γ-TiAl. Thus, γ-TiAl is a representative intermetallic compound that includes three totally different stress–strain modes. We demonstrate that all the structure transitions in the FPCTT and FPCCT result from the breakage or formation of bonds, and this can be generalized to all the structural transitions. Furthermore, based on the calculations we qualitatively show that the Ti–Al bond should be stronger than the Ti–Ti bond in γ-TiAl. Our results provide a useful reference for understanding the intrinsic bonding and mechanical properties of γ-TiAl as a high-temperature structural material.

(Some figures in this article are in colour only in the electronic version)

1. Introduction

Of all the TiAl-based intermetallic compounds, γ-TiAl is the most promising as a high-temperature candidate that can be used in aerospace engine components because of its excellent equilibrium in density, strength and high-temperature oxidation resistance [1–4]. Extensive studies of γ-TiAl have been made since the 1980s, particularly of its intrinsic electronic structure, interatomic bonding, grain boundaries, impurity and alloying elements, as well as their effects on mechanical properties [5–17]. The room-temperature brittleness, however, is a factor that seriously limits its application. Such brittleness is directly related to the intrinsic bonding properties of γ-TiAl.

In order to further investigate the intrinsic bonding and mechanical properties of γ-TiAl, in this paper we calculate the theoretical tensile and compressive strength of γ-TiAl using a first-principles computational tensile/compressive test (FPCTT/FPCCT) [18–45]. The maximum stress which can break a pure crystal (either tensile or compressive) is considered to be the theoretical (ideal) strength (tensile or compressive) of the crystal [46–48]. The theoretical strength can be calculated using a first-principles method [49], and such a method has successfully been applied to both single crystals [18–45] and grain boundaries [50–55].

For intermetallics, several FPCTT/FPCCT studies have been performed so far on the $B2$ (NiAl, FeAl, and CoAl) [18, 34], $D0_{22}$ and $L1_2$ (Al_3Ti, Al_3V and Al_3Sc) [38, 43]

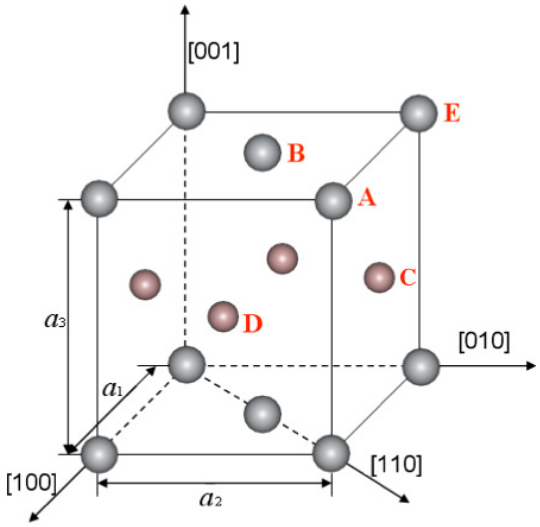

Figure 1. A unit cell of γ-TiAl with the $L1_0$ structure. Different crystalline directions are shown. The smaller pink spheres denote Al atoms, and the larger gray spheres denote Ti atoms. Atoms denoted by A, B, C, D, and E are discussed later.

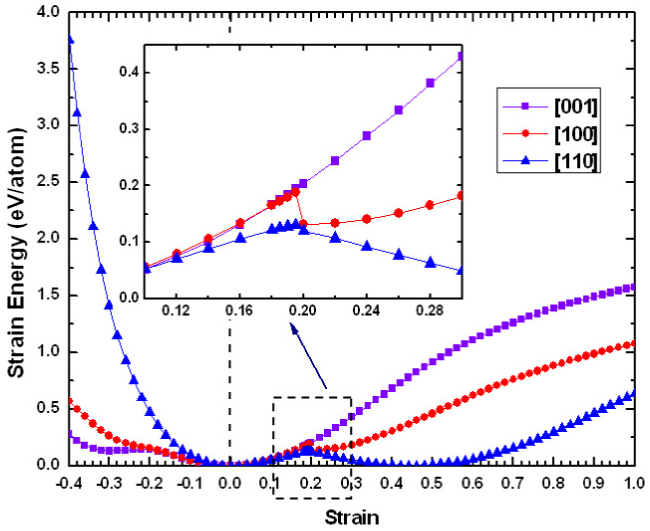

Figure 2. The strain energy as function of uniaxial deformation for γ-TiAl in the [001], [100] and [110] directions. The inside panel is an enlargement for clarity of the rectangular part shown in the outside panel in the strain range from 0.10 to 0.30.

structures. Few studies, however, have focussed on the $L1_0$ structure intermetallics, including TiAl, FePt, and CuAu, which have a distinct characteristic quite different from those with other structures such as $B2$, $D0_{22}$ and $L1_2$. For instance, the c/a ratio of the $L1_0$-structure TiAl (figure 1) is about 1.02 for γ-TiAl, which makes it exhibit an obvious anisotropy in different crystalline directions. According to the crystalline structure of γ-TiAl, the [001], [100] {or [010]} and [110] directions are typically anisotropic. Such anisotropy can be intrinsically reflected in the corresponding theoretical strength as well as the stress–strain relationship.

The theoretical strength in a certain crystalline direction reveals the intrinsic bonding characteristic relating to that direction. Calculating the theoretical strength of γ-TiAl in different directions can provide an insight into its intrinsic bonding characteristic. Further, the strengths of Ti–Ti and Ti–Al bonds can be obtained based on the FPCTT/FPCCT results, which can qualitatively show which bond is more covalent. Our results provide a good reference for understanding the intrinsic bonding and mechanical properties of γ-TiAl, and are thus helpful for understanding the origin of room-temperature brittleness.

2. Computational method

We employ a first-principles plane-wave total energy method based on density functional theory with the generalized gradient approximation according to Perdew and Wang [56] using VASP [57–59]. The ion–electron interaction is described by the ultrasoft pseudopotential. The energy cutoff for the plane-wave basis was chosen to be 355 eV. The k-point was sampled by a (12 × 12 × 11) grid according to the Monkhorst–Pack scheme [60] corresponding to the optimized lattice constants of the unit cell (0.3985 nm × 0.3985 nm × 0.4076 nm), which are lower than the experimental value by about 0.01 [61]. The optimized c/a is 1.023.

The FPCTT/FPCCT was done by a series of strains applied to the unit cell in order to get the response of the employed unit cell to uniaxial tensile and compressive deformation along the selected path for γ-TiAl. The selected unit cell is fully relaxed at each deformation step until the forces on all the atoms are converged to less than 10^{-3} eV Å^{-1}, and the total energy as well as the stress as a function of uniaxial strain can thus be obtained.

In the FPCTT/FPCCT, the Hellmann–Feynman theorem is adopted to determine the tensile stress through the Nielsen–Martin scheme [62], according to which the stress $\sigma_{\alpha\beta}$ can be calculated from

$$\sigma_{\alpha\beta} = \frac{1}{\Omega}\frac{\partial E_{\text{total}}}{\partial \varepsilon_{\alpha\beta}}, \tag{1}$$

where $\varepsilon_{\alpha\beta}$ is the strain tensor ($\alpha, \beta = 1, 2, 3$), and Ω is the volume of the unit cell.

3. FPCTT of γ-TiAl in different directions

A uniaxial tensile/compressive strain was applied in the [001], [110] and [100] directions, respectively. Figures 2 and 3 show the energies and the stresses as a function of strain in the [001], [110] and [100] directions for both FPCTT (right part) and FPCCT (left part).

3.1. FPCTT in the [001] direction

The [001] direction is the most symmetric path for γ-TiAl. The unit cell we used in the calculation for this direction is the face-centered tetragonal (fct) structure, as shown in figure 1. The lattice parameters for the unit cell are

$$a_1 = a_0, \qquad a_2 = a_0, \qquad a_3 = 1.023a_0, \tag{2}$$

where a_0 is the unit length of a_1 and a_2, i.e. 0.3985 nm.

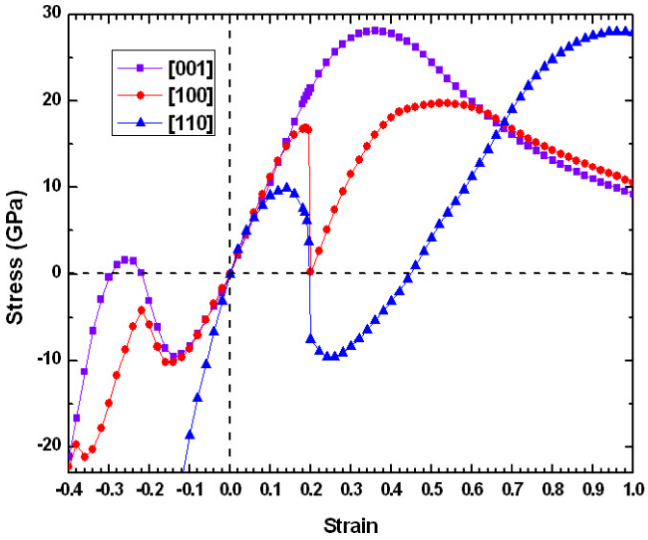

Figure 3. The stress as a function of tensile and compressive deformation for γ-TiAl in the [001], [100] and [110] directions.

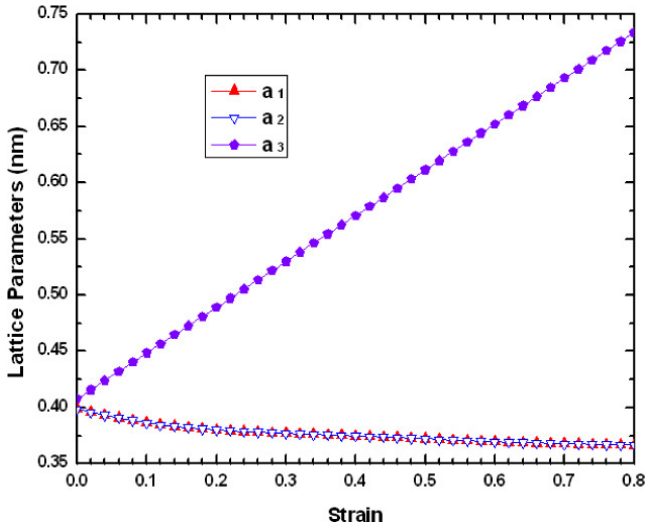

Figure 4. Lattice parameters of a1, a2 and a3 as a function of strain along [001].

All the planes parallel to the [001] direction are fully identical, indicating that there is only one kind of bond, i.e. Ti–Al, in the tensile direction. This suggests that smooth plots of energy and stress as a function of linear extension would be obtained.

The energy per atom as a function of tensile strain is shown in figure 2. The energy increases with increasing tensile strain, but exhibits an inflexion at a strain of 0.36. Correspondingly, the tensile stress increases with increasing tensile strain until a strain of 0.36, at which the stress reaches a maximum, as shown in figure 3. After 0.36, the stress decreases gradually. Hence, the maximum stress of 28.1 GPa is the theoretical tensile strength in the [001] direction.

Lattice parameters as a function of strain in the tensile process along the [001] direction are shown in figure 4. The lattice parameter of a_3 increases, while a_1 and a_2 are always equal under [001] uniaxial loading, which implies that the tetragonal symmetry of the present unit cell remains unchanged under uniaxial tensile stress.

3.2. FPCTT in the [110] direction

For calculational convenience, we used the body-centered tetragonal (bct) structure of γ-TiAl with two atoms in the unit cell to perform FPCTT in the [110] direction, as shown in figure 5. The bct structure is equivalent to the fct structure in figure 1. The initial lattice parameters for the bct structure are

$$b_1 = \frac{\sqrt{2}}{2}a_0, \qquad b_2 = \frac{\sqrt{2}}{2}a_0, \qquad b_3 = 1.023a_0. \quad (3)$$

The k-point mesh under the Monkhorst–Pack scheme increases correspondingly for the bct unit cell due to the reduced lattice parameters in comparison with the fct unit cell.

The results for the energy–strain relationship in the [110] direction are displayed in figure 2. There is one energy maximum and one energy minimum (zero energy state) in the energy–strain curve, corresponding to the two stress-free states in the stress–strain curve in figure 3. The stress reaches a maximum tensile stress of 9.89 GPa and a maximum negative stress of −9.6 GPa at a strain of 0.14 and 0.24, respectively. However, such negative stress from the strain of 0.20–0.44 is not compressive physically. The energy corresponding to this negative 'virtual' stress range decreases with the increasing strain, as shown in figure 2, and it occurs only when the strain is applied on the system discontinuously. A similar phenomenon also occurs on Mo, Nb, Gum Metals and Al_3 (Sc, Ti, V) systems [24, 31, 41, 43].

Originally, the unit cell of the TiAl crystal is of a tetragonal structure, with $b_1 = b_2 \neq b_3$ (we call this structure bct-I), as shown in figure 6. Applying strain on the unit cell leads to an increase in b_1 and decreases in b_2 and b_3 due to the role of the Poisson ratio. The tetragonal symmetry is destroyed when the unit cell deviates from the starting state due to the strain increase. However, b_1, b_2 and b_3 remain perpendicular to each other and thus the unit cell exhibits an orthorhombic symmetry. The length of b_3 becomes equal to that of b_1 at a strain of 0.19, leading to the appearance of the first stress-free structure. The saddle point structure with $b_1 = b_3 \neq b_2$ forms at this strain (bct-II), as shown in figure 6. The tetragonal symmetry restores at this strain point. Such a bct-II structure is unstable, since the energy exhibits a maximum and decreases with further strain increase until a strain of 0.45. Further strain increase will not destroy such tetragonal symmetry, but the lattice parameters of the unit cell become $b_2 = b_3 \neq b_1$. The other stress-free state appears at a strain of ∼0.45 (bct-III), corresponding to the ground-state zero strain energy point.

This path is well known as the 'orthorhombic' path, which is similar to previous studies on Mo and Nb [24]. The lattice parameters for bct-III are exactly the same as the original ones without applied strain, but with a 90° rotation. As a matter of fact, the TiAl crystal can be considered to be pulled along the original [001] direction after bct-III appears, resulting in a similar energy–strain and stress–strain relationship as that in

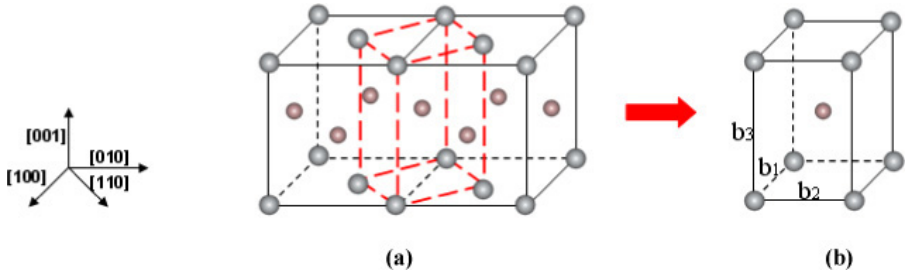

Figure 5. The face-centered tetragonal (fct) crystal in (a) can also be treated as body-centered tetragonal (bct) as indicated by the red dashed part. (b) Such a bct structure, in which the lattice parameters are denoted by b_1, b_2 and b_3.

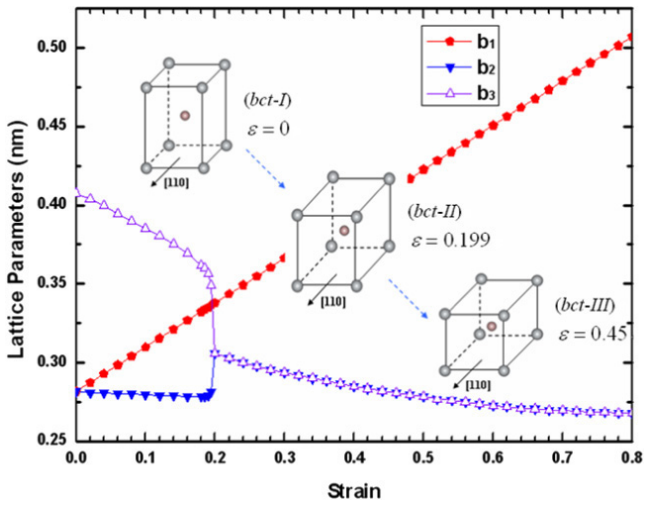

Figure 6. Lattice parameters and evolution of geometric structure as a function of tensile strain in the [110] direction. The structure evolves as bct-I → bct-II → bct-III, as shown in the three inside panels.

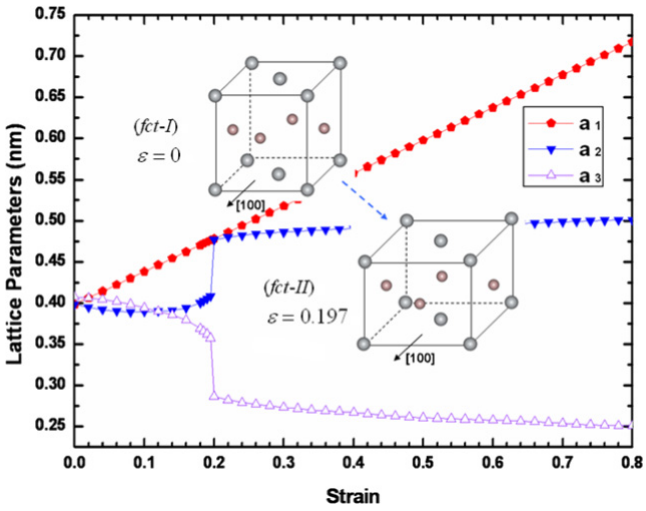

Figure 7. Lattice parameters and evolution of geometric structures as a function of tensile strain in the [100] direction. The phase evolves as fct-I → fct-II, as shown in the two inside panels.

the [001] direction in figure 3. The TiAl crystal experiences a stable–unstable–stable (bct-I → bct-II → bct-III) transition process with the applied uniaxial strain in the [110] direction.

The theoretical tensile strength corresponds to the first maximal stress before the saddle point structure appears in the stress–strain curve [34], which can give us very important information about the intrinsic mechanical properties of γ-TiAl. For the [110] direction, the theoretical tensile strength for γ-TiAl along [110] is 9.9 GPa at a strain of 0.14. Compared with the theoretical tensile strength of 28.1 GPa in the [001] direction, the theoretical tensile strength in [110] is much lower, which indicates that [110] in γ-TiAl is a weak crystalline direction under tensile strain.

3.3. FPCTT in the [100] direction

For the FPCTT in the [100] direction we used the fct unit cell again shown in figure 1, the same as that in the [001] direction. Figure 2 demonstrates that the energy increases initially with increasing strain, and exhibits a maximum at a strain of 0.19. This corresponds to the stress maximum of 16.9 GPa in the stress–strain curve (figure 3). The stress goes quickly to zero when the strain is larger than ∼0.19, suggesting that a phase transition occurs here. The energy reduces as well, indicating that the system becomes stable. From a strain of 0.20, the stress as well as the energy increased with further increase in strain, but the stress meets another maximum of 19.7 GPa at a strain of 0.54.

In the tensile process in the [100] direction, a phase transition occurs which is quite different from that of both the [001] and [110] directions. The initial geometry of the unit cell is of tetragonal symmetry with the lattice parameters shown in equation (2). Further increase in strain changes the symmetry from tetragonal to orthorhombic. The initial tetragonal symmetry goes back instantaneously at a strain of ∼0.20, with the crystal structure of

$$a_1 = 1.2a_0, \qquad a_2 = 1.2a_0, \qquad a_3 = 0.72a_0, \quad (4)$$

in which a_1 is equal to a_2 again, and a_3 is about one-third shorter than both a_1 and a_2. This is quite different from the initial phase despite both exhibiting the fct structure. In the initial phase, a_3 is a bit longer than both a_1 and a_2. Here, we call the initial fct phase fct-I, while the fct phase corresponding to equation (4) is fct-II. Figure 7 shows the lattice parameters as a function of strain and such a phase transition process.

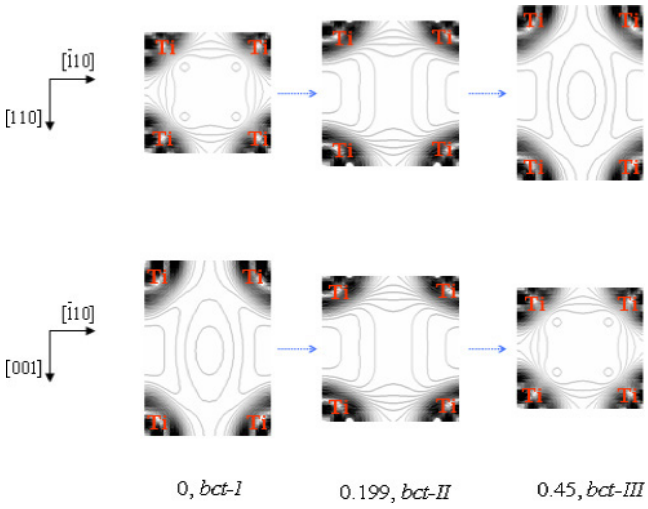

Figure 8. The evolution of charge distribution between the Ti atoms in the bct crystal under tension along the [110] direction. The upper panel shows the charge distribution of (001), and the lower panel shows those of (110).

4. Anisotropy of theoretical tensile strength and stress–strain relation

According to the above analysis, we found interestingly that the stress–strain relations and the theoretical tensile strength for the respective direction due to the applied tensile strain are totally different, as shown in figure 3. The theoretical tensile strength of [001] is ∼28 GPa, which is the highest one in comparison with those of the other two directions, while [110] is the weakest direction with a tensile strength of ∼10 GPa. Such differences originate from the structural anisotropy in the three different directions of γ-TiAl.

Only the Ti–Al bonds exist in the plane parallel to the [001] tensile direction. Thus, the Ti–Al bond dominates the stress–strain relation in the [001] direction. The theoretical tensile strength also characterizes the intrinsic bond strength of Ti–Al despite the deviation of the Ti–Al bond from the tensile direction by nearly 45°. The stress–strain curve exhibits only one stress maximum because the symmetry stays the same and no structural transition occurs.

The lattice parameter in the [110] tensile direction is shorter than any of the other two directions, as shown in equation (3), for which the bct-I → bct-II → bct-III structure transitions occur. The first transition of bct-I → bct-II is characterized by a break of the Ti–Ti bond in the tensile direction, while the second transition of bct-II → bct-III is characterized by a recombination of the Ti–Ti bond normal to the tensile direction. This point can be confirmed by the charge density distribution between the Ti atoms as a function of strain, as shown in figure 8. The charge density of the Ti–Ti bonds in the tensile direction becomes extremely small for bct-II, while that of the Ti–Ti bonds normal to the tensile direction accumulates again for bct-III. The formation of the 'stress-free' structure should be dominated by the corresponding bond breakage or combination. *This suggests that bond breakage or formation plays a key role in the structural transition.*

Now let us see how bond breakage leads to the fct-I → fct-II phase transition in the [100] direction. One may note that there also exist three kinds of atomic bonds, i.e. Ti–Ti, Al–Al and Ti–Al. For convenience, let AB and CD represent Ti–Ti and Al–Al bonds, respectively, and let AC and AD represent the Ti–Al bond which is in the crystalline plane parallel and perpendicular to the tensile direction, respectively. These letters are clearly denoted in figure 1.

Figure 9 shows the bond length as a function of strain, including four typical bonds of AB, CD, AC and AD. The CD bond (Al–Al) exhibits the same trend as AB (Ti–Ti) with increasing strain since Al–Al is much weaker due to its metallic characteristic in comparison with Ti–Ti containing covalent character. Both AB and AC increase first with increasing strain, but AB changes abruptly at the strain of 0.195, while AC decreases, indicating the AB break. The length of the AB bond is ∼0.31 nm at this strain. Such bond breakage leads directly to a phase transition to fct-II. This is similar to the phase transition in the tensile process for ZnO with a one-dimensional nanostructure [63]. The charge density distribution plots demonstrate the bond break in the phase transition from fct-I to fct-II, as shown in figure 10.

The structural anisotropy also results in the different stress–strain relations in the different directions. No saddle point appears in the [001] direction, and the stress–strain curve exhibits only one stress maximum. This is a general mode for the FPCTT of the single crystal [18–20, 22, 23, 26, 27, 29, 32, 34, 36, 38–40, 42, 44, 45]. The stress–strain curve in [110] represents a typical mode of the 'orthorhombic path' with the saddle point structure and two stress maxima [24, 31, 41, 43]. The 'Bain path' (bcc–fcc structure transition) is actually a special case of the 'orthorhombic path'. The structure of the [100] direction leads to a one-phase-transition and two-stress-maxima stress–strain curve, which is a special stress–strain mode. However, the 'double stress maxima' phenomenon concerning the Al grain boundary [52–55, 64, 65] can also be attributed to this mode. All three of these modes appear together in γ-TiAl, making it a representative crystal for investigating anisotropy of the theoretical strength and stress–strain relation.

5. FPCCT of γ-TiAl

As shown in figure 3, compressive strain led to two structure transitions, including a saddle point structure in the stress–strain relation in the [001] direction and ever-increasing compressive stress as a function of strain in the [110] direction without any structure transition, opposite to that occurring in the FPCTT in the same direction. For the [100] direction, there appears a stress–strain relation different from the FPCTT stress–strain curve in the same direction.

For the FPCCT in the [001] direction, we use a fct unit cell again, as shown in figure 1. The energy as a function of strain (the left part of figure 2) shows that the strain energy increases initially with increasing compressive strain, and exhibits a local maximum at a strain of −0.22. After this point, the strain energy decreases following the increase in strain, and exhibits a local minimum at a strain −0.30. Thus, one energy maximum

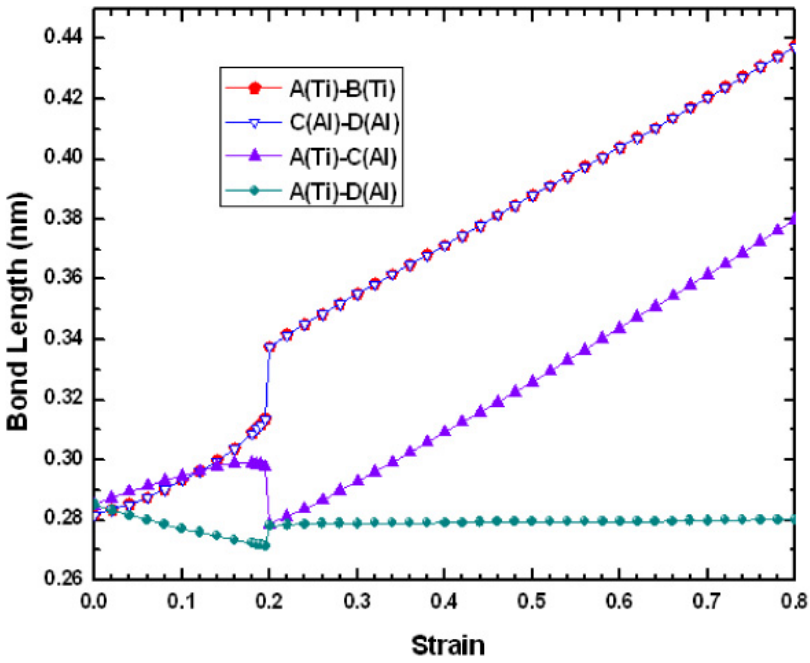

Figure 9. The length evolution of representative bonds with increasing strain under a uniaxial tensile strain applied in the [100] direction.

Table 1. The stress maxima and the corresponding strains in the tensile and compressive process. The bold italic values in the table indicate the theoretical tensile or compressive strengths in the respective directions.

Crystalline direction	Stress maxima in tension				Stress maxima in compression			
	First		Second		First		Second	
	ε	σ (GPa)	ε	σ (GPa)	ε	σ (GPa)	ε	σ (GPa)
[001]	0.36	***28.1***	—	—	−0.14	***−9.6***	—	—
[110]	0.14	***9.9***	0.96	28.0	—	—	—	—
[100]	0.19	***16.9***	0.54	19.7	−0.16	***−10.2***	−0.36	−21.1

and one energy minimum appear in the energy–strain curve, corresponding to the two stress-free structures in the stress–strain curve in the left part of figure 3. The stress reaches a maximum compressive stress of −9.59 GPa and a maximum 'tensile' (i.e. positive) stress of 1.61 GPa at strains of −0.14 and −0.26, respectively.

The lattice parameters in the zero strain state are shown in equation (2). Compressive strain leads to a decrease of the lattice parameter in the compressive [001] direction and an increase in other two directions. At a strain of −0.22, the lattice parameters become

$$a_1 = 1.13a_0, \qquad a_2 = 1.13a_0, \qquad a_3 = 0.8a_0, \qquad (5)$$

which exhibits a stress-free $B2$ structure, characterized by a_1 being equal to a_2, and a_3/a_1 is $\sim\sqrt{2}/2$. Further compression results in the formation of another stress-free $L1_0$ structure at a strain of −0.30 as expressed in equation (4) (i.e. the same as 'fct-II'). Therefore, the two stress-free points correspond to the $B2$ and 'fct-II' structure, respectively. The theoretical compressive strength of the [001] direction is 9.59 GPa at the compressive strain of 0.14, which is the first compressive stress maximum before the stress-free structure appears.

The fct unit cell has been used again for compression in the [100] direction. Figure 11 shows the change of the lattice parameters and the bond length with increasing strain. Compression in the [100] direction makes the original Ti–Ti bonds (AB in figure 1) shrink gradually until a strain of −0.16, where the bond length of these Ti–Ti bonds becomes shortest. The original increase in compressive stress is caused by the contraction of these Ti–Ti bonds. From the strain of −0.16, these Ti–Ti bonds start to extend, leading to the formation of a stress maximum (−10.21 GPa) at this strain and the stress decrease. At a strain of −0.22, the Ti atoms of A and E (figure 1) bond with each other, leading to an increase in compressive stress from this strain. The stress corresponding to this strain is −4.23 GPa. Moreover, there appears an additional stress peak at a strain of −0.36, which is possibly related to the Al–Al bonds. It should be noted that no saddle point structure forms in the whole compression process in the [100] direction according the above discussion and the energy–strain curve (figure 2).

For the [110] direction, we use a bct unit cell as shown in figure 5 to perform the FPCCT. Both Ti–Ti and Al–Al bonds exhibit the equilibrium bond length along the [110] direction without compression. Consequently, the stress increases rapidly with increasing compressive strain, corresponding to the energy increase as a function of strain, as shown in figures 2 and 3 (left part). The compressive strength in this direction should be larger than that in the [001] and [100] directions.

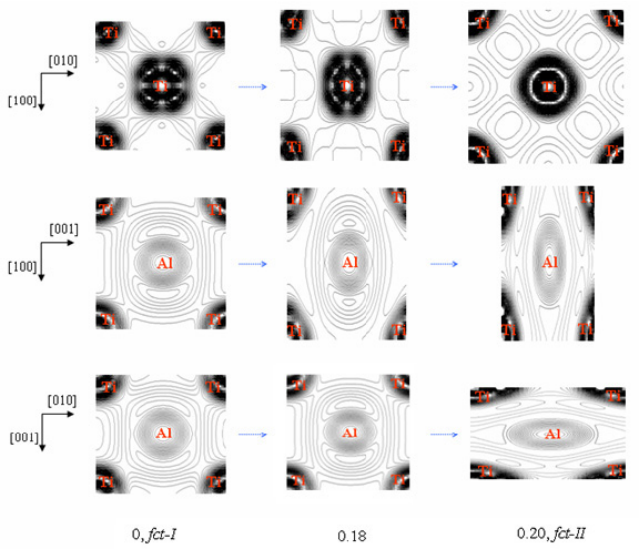

Figure 10. The evolution of charge distribution of Ti–Ti and Ti–Al bonds under tension along the [100] direction. The upper, middle and lower panels show the charge distribution of (001), (010) and (100) crystalline planes, respectively.

All the maximum stresses and the corresponding strains in different directions for FPCTT and FPCCT are listed in table 1 for comparison.

6. Which is stronger, Ti–Ti or Ti–Al?

It is generally considered that the room-temperature brittleness of TiAl originates in its intrinsic atomic bonding with directional covalent components. According to the electronic structure calculation of Morrinaga *et al* [6], the brittleness was suggested to originate from the Al(3p)–Ti(3d) directional bonding containing covalent component, while Song *et al* [7] concluded that both Ti(3d)–Ti(3d) and Al(3p)–Ti(3d) bonding are directional and covalent, and thus responsible for the brittleness. In the following, we will show which bond is stronger based on the FPCTT and FPCCT results.

On the one hand, we can qualitatively analyze the strength of the Ti–Ti and Ti–Al bonds according to the evolution of the bond length shown in figure 9. Originally, with increasing strain, the stress applies to both the Ti–Ti bonds in the (001) plane and the Ti–Al bonds in the (010) and (020) planes as well as the Al–Al bonds in the (002) plane. Figure 9 shows that both the Ti–Ti and Al–Al bonds extend rapidly at a strain of 0.195, while the Ti–Al bond contracts, implying the breaking of both Ti–Ti and Al–Al bonds. If simply considering that the weaker bond should break first with the same applied stress, this suggests that the Ti–Ti bond is weaker than the Ti–Al one. The Al–Al bond should be much weaker due to its metallic characteristics. It exhibits the same trend as the Ti–Ti bond because it shares the same plane as the Ti–Ti bond, which limits its extension.

On the other hand, the stress–strain relation in the [100] direction leads to the same conclusion. As discussed in section 5, the first stress maximum is ∼17 GPa, characterized

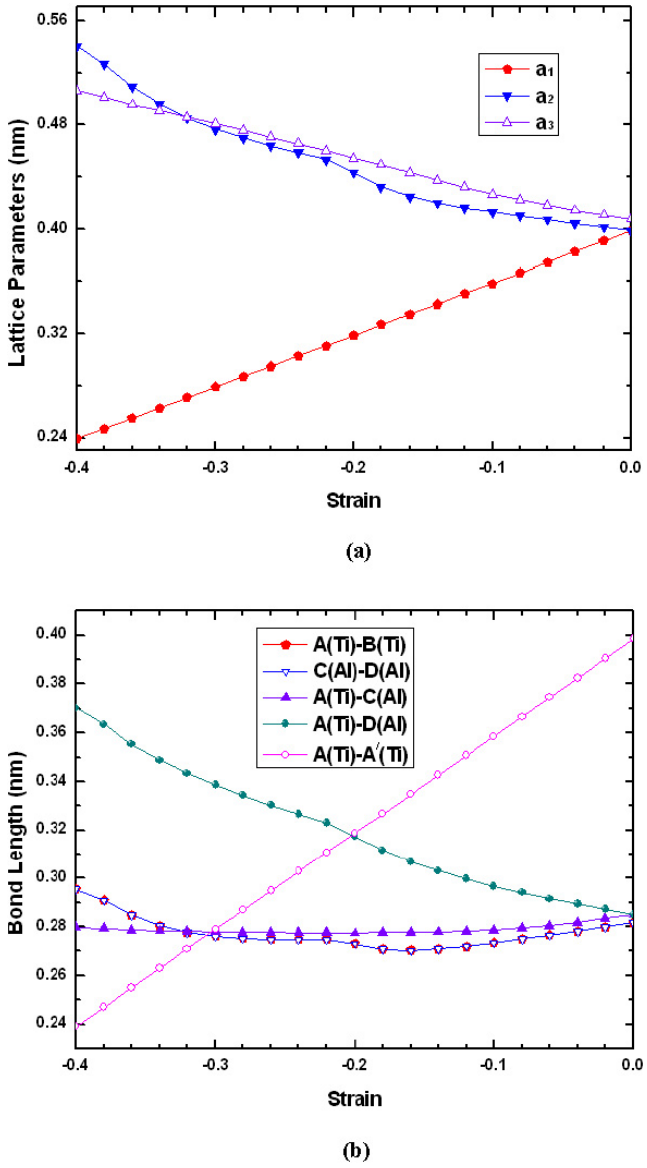

Figure 11. Lattice parameters (a) and bond lengths (b) as a function of compressive strain in the [100] direction.

by the breakage of the Ti–Ti bond after this. The second stress maximum is ∼20 GPa, characterized by the Ti–Al bond starting to break. Because (i) Ti–Ti has almost the same angle with respect to the tensile direction as Ti–Al (about 45°) and (ii) Ti–Ti and Ti–Al are in two different planes perpendicular to each other, the first stress maximum should represent the strength of both the Ti–Ti and Ti–Al bonds. Here, as mentioned above, the Al–Al bonds should be very weak compared with Ti–Ti and Ti–Al and thus has been not considered. The second stress maximum represents the strength of the Ti–Al bond since only Ti–Al bonds are left provided the Ti–Ti bond has broken. Note there are four Ti–Ti bonds in the (001) plane and eight Ti–Al bonds in the (010) and (020) planes. On average we can estimate that the strength of the Ti–Ti bond is ∼1.4 GPa according to the first maximum with 12 bonds of Ti–Ti and Ti–Al together, and that for the Ti–Al bond is ∼2.5 GPa according to the second maximum with eight Ti–Al bonds. This indicates that the Ti–Al bond should be stronger

than the Ti–Ti bond. Similarly, from the first and second stress maxima in the [110] direction one can also reach the same conclusion. However, both Ti–Al and Ti–Ti bonds contain the covalent components and thus the brittleness should be related not only to the stronger Ti–Al bond.

7. Comparison with other intermetallics

For intermetallics, several FPCTT/FPCCT studies have so far been performed on the $B2$ (NiAl, FeAl and CoAl) [18, 34], $D0_{22}$ and $L1_2$ (Al_3Ti, Al_3V and Al_3Sc) [38, 43] structures. The FPCTT of $B2$ transition-metal aluminides has been done [18, 34]. Sob *et al* [18] studied the ideal tensile strength of NiAl pulled in [100] and [111] directions, while Li *et al* [34] investigated the ideal strengths of the $B2$-type transition-metal aluminides including NiAl as well as FeAl and CoAl along [001], [110] and [111] directions. It should be pointed out that those three materials exhibit different tensile strengths under the FPCTT. NiAl and CoAl are strongest in the [001] direction, while FeAl is the weakest in the same direction. Antibonding d states are suggested to be responsible for the weakness of FeAl along this direction.

The same FPCTTs have been performed on Al_3TM (transition metal) with the $L1_2$ and $D0_{22}$ crystal structure, including Al_3Ti, Al_3V and Al_3Sc by Jahnatek *et al* [38, 43]. The Al–Ti and Al–V bonds are shown to exhibit a characteristic feature of covalent bonding from the charge distribution. Different behaviors of $L1_2$ and $D0_{22}$ structures under FPCTT are discussed in detail. The theoretical strength of these intermetallics in different directions has been fully compared. Moreover, the theoretical strengths of both Al_3V and Al_3Ti are much higher than that of the respective pure materials (i.e. fcc-Al and bcc-V).

As mentioned above, little work has so far been done on $L1_0$ structure intermetallics such as γ-TiAl. Comparing the strength of γ-TiAl with the corresponding strength of Al_3Ti, for example, can lead to some useful conclusions. For example, the [001] direction exhibits much higher (>0.40) theoretical tensile strength (∼28 GPa) than the [100] direction (∼17 GPa). Because the symmetries in the [001] and [100] directions are exactly the same, we are able to compare the theoretical tensile strengths in these two directions. The theoretical tensile strength in the [001] direction is contributed by all the Ti–Al bonds in the four crystalline planes (per cell) parallel to this direction. On the other hand, the theoretical tensile strength in the [100] direction is also contributed by the four crystalline planes parallel (per cell) to this direction, but consisting of two with Ti–Al bonds, one with Ti–Ti bonds and one with Al–Al bonds. The effect of the Al–Al bond plane can be estimated by comparison of the theoretical tensile strength of TiAl in [001] with that of $L1_2$-$TiAl_3$ in the same direction. The theoretical tensile strength of $L1_2$-$TiAl_3$ in [001] is ∼20 GPa according to the previous study [38], but consisting of two Al–Al and two Ti–Al bond planes (per cell). Thus, approximately one Al–Al bond plane will reduce the tensile strength of ∼4 GPa, which shows the Al–Al bond is very weak in comparison with the Ti–Al bond[4].

[4] We can make such a comparison because we use the same code and similar computational conditions such as cutoff energy and k-points.

8. Summary

We perform first-principles computational tensile and compressive tests (FPCTT and FPCCT) to investigate the intrinsic bonding and mechanical properties of the γ-TiAl intermetallic compound with the $L1_0$ structure using a first-principles total energy method. The stress–strain relations and the corresponding theoretical tensile strengths are found to be characteristic in the [001], [100] and [110] crystalline directions, as a result of the structural anisotropy in these directions. In the FPCTT, the [001] direction exhibits only one stress maximum and no structural transition, and the [110] direction exhibits two stress maxima and two structural transitions, while the [100] direction exhibits two stress maxima with the phase transition. The tensile strengths are 28.9, 9.9 and 16.9 GPa in the [001], [110] and [100] directions, respectively. Differently, in the FPCCT, the [100] direction exhibits two stress maxima, and the [001] direction exhibits only one, while the [110] direction exhibits no stress maxima. γ-TiAl is thus a representative intermetallic compound exhibiting three totally different stress–strain modes. We demonstrate that all the structural transitions in the FPCTT and FPCCT result from bond breakage or formation, which can be generalized to all the structural transitions. Furthermore, the Ti–Al bond is qualitatively shown to be stronger than the Ti–Ti bond and thus contains more covalent character in the γ-TiAl intermetallic compound according to the calculation results. Our study provides a useful reference for understanding the intrinsic bonding and mechanical properties of γ-TiAl.

Acknowledgments

The research is supported by Aeronautics Science Foundation of China (ASFC) with grant no. 2007ZF51071 and New Century Excellent Talents in University with grant no. NCET-07-0040.

References

[1] Kim Y W and Miner J 1994 *Met. Mater. Soc.* **46** 30
[2] Yamaguchi M and Umakoshi Y 1990 *Prog. Mater. Sci.* **34** 1
[3] Yamaguchi M, Inui H and Ito K 2000 *Acta Mater.* **48** 307
[4] Loria E A 2001 *Intermetallics* **9** 997
[5] Greenberg B F, Anisimov V I, Gornostirev Y N and Taluts G G 1988 *Scr. Metall.* **22** 859
[6] Morinaga M, Satio J, Yukawa N and Adachi H 1990 *Acta Metall. Mater.* **38** 25
[7] Song Y, Tang S P, Xu J H, Mryasov O N, Freeman A J, Woodard C and Dimiduk D M 1994 *Phil. Mag.* B **70** 987
[8] Simmons J P, Rao S I and Dimiduk D M 1998 *Phil. Mag. Lett.* **77** 327
[9] Mryasov O N, Gornostyrev Y N and Freeman A J 1998 *Phys. Rev.* B **58** 11927
[10] Appel F 2001 *Mater. Sci. Eng.* A **317** 115
[11] Zhang W J, Reddy B V and Deevi S C 2001 *Scr. Mater.* **45** 645
[12] Hsiung L, Nieh T, Choi B W and Wadaworth J 2002 *Mater. Sci. Eng.* A **329** 637
[13] Mishin Y and Herzig C 2002 *Acta Mater.* **48** 589
[14] Song Y, Guo Z X and Yang R 2002 *J. Light Met.* **2** 115
[15] Yu R, He L L and Ye H O 2002 *Phys. Rev.* B **65** 184102
[16] Zope R R and Mishin Y 2003 *Phys. Rev.* B **68** 024102

[17] Dang H L, Wang C Y and Yu T 2007 *J. Appl. Phys.* **101** 083702
[18] Sob M, Wang L G and Vitek V 1998 *Phil. Mag.* B **78** 653
[19] Ogata S and Kitagawa H 1999 *Comput. Mater. Sci.* **15** 435
[20] Krenn C R, Roundy D, Morris J W Jr and Cohen M L 2001 *Mater. Sci. Eng.* A **319–321** 111
[21] Roundy D, Krenn C R, Cohen M L and Morris J W Jr 2001 *Phil. Mag.* A **81** 1725
[22] Roundy D and Cohen M L 2001 *Phys. Rev.* B **64** 21 2103
[23] Ogata S, Hirosaki N, Kocer C and Kitagawa H 2001 *Phys. Rev.* B **64** 172102
[24] Luo W D, Roundy D, Cohen M L and Morris J W Jr 2002 *Phys. Rev.* B **66** 094110
[25] Clatterbuck D M, Chrzan D C and Morris J W Jr 2002 *Phil. Mag. Lett.* **82** 141
[26] Clatterbuck D M, Krenn C R, Cohen M L and Morris J W Jr 2003 *Phys. Rev. Lett.* **91** 135501
[27] Kocer C, Hirosaki N and Ogata S 2003 *Phys. Rev.* B **67** 035210
[28] Cerny M, Pokluda J and Sob M 2003 *Phys. Rev.* B **67** 035116
[29] Ogata S and Shibutani Y 2003 *Phys. Rev.* B **68** 165409
[30] Friak M, Sob M and Vitek V 2003 *Phys. Rev.* B **68** 184101
[31] Clatterbuck D M, Chrzan D C and Morris J W Jr 2003 *Acta Mater.* **51** 2271
[32] Clatterbuck D M, Chrzan D C and Morris J W Jr 2003 *Scr. Mater.* **49** 1007
[33] Friak M, Sob M and Vitek V 2003 *Phil. Mag.* **83** 3529
[34] Li T S, Morris J W Jr and Chrzan D C 2004 *Phys. Rev.* B **70** 054107
[35] Cerny M, Sob M, Pokluda J and Sandera P 2004 *J. Phys.: Condens. Matter* **16** 1045
[36] Ogata S, Hirosaki N and Kocer C 2004 *Acta Mater.* **52** 233
[37] Sob M, Friak M, Legut D, Fiala J and Vitek V 2004 *Mater. Sci. Eng.* A **387–389** 148
[38] Jahnatek M, Krajci M and Hafner J 2005 *Phys. Rev.* B **71** 024101
[39] Liao T, Wang J Y and Zhou Y C 2006 *Phys. Rev.* B **74** 174112
[40] Liao T, Wang J Y and Zhou Y C 2006 *Phys. Rev.* B **73** 214109
[41] Li T S, Morris J W Jr, Nagasako N, Kuramoto S and Chrzan D C 2007 *Phys. Rev. Lett.* **98** 105503
[42] Yu R, Zhang X F, De Jonghe L C and Ritchie R O 2007 *Phys. Rev.* B **75** 104114
[43] Jahnatek M, Krajci M and Hafner J 2007 *Phys. Rev.* B **76** 014110
[44] Zhang Y, Sun H and Chen C F 2007 *Phys. Rev.* B **76** 144101
[45] Jindo K M, Hung V V, Hoa N T and Turchi P E A 2008 *J. Alloys Compounds* **452** 127
[46] Kelly A and Macmillan N H 1986 *Strong Solids* 3rd edn (Oxford: Clarendon) p 6
[47] Morris J W Jr and Krenn C R 2000 *Phil. Mag.* A **80** 2827
[48] Morris J W Jr, Krenn C R, Roundy D and Cohen M L 2000 *Phase Transformations and Evolution in Materials* (Warrendale, PA: TMS) p 187
[49] Morris J W Jr and Krenn C R 2000 *Phil. Mag.* A **80** 2827
[50] Kohyama M 1999 *Phil. Mag. Lett.* **79** 659
[51] Kohyama M 2002 *Phys. Rev.* B **65** 184107
[52] Lu G H, Deng S H, Wang T M, Kohyama M and Yamamoto R 2004 *Phys. Rev.* B **69** 134106
[53] Lu G H, Zhang Y, Deng S H, Wang T M, Kohyama M, Yamamoto R, Liu F, Horikawa K and Kanno M 2006 *Phys. Rev.* B **73** 224115
[54] Zhang Y, Lu G H, Wang T M, Deng S H, Kohyama M and Yamamoto R 2006 *Mater. Trans.* **47** 2678
[55] Zhang Y, Lu G H, Deng S H, Wang T M, Xu H B, Kohyama M and Yamamoto R 2007 *Phys. Rev.* B **75** 174101
[56] Lue C S, Chepin S, Chepin J and Ross J H Jr 1998 *Phys. Rev.* B **57** 7010
[57] Kresse G and Hafner J 1993 *Phys. Rev.* B **47** 558
[58] Kresse G and Furthmüller J 1996 *Phys. Rev.* B **54** 11169
[59] Kresse G and Furthmüller J 1996 *Comput. Mater. Sci.* **6** 15
[60] Monkhorst H J and Pack J D 1976 *Phys. Rev.* B **13** 5188
[61] Pearson W B 1987 *A Handbook of Lattice Spacing and Structure of Metal and Alloys* vol 1–2 (Oxford: Pergamon)
[62] Nielsen O H and Martin R M 1985 *Phys. Rev.* B **32** 3780
Nielsen O H and Martin R M 1987 *Phys. Rev.* B **35** 9308
[63] Kulkarni A J, Zhou M and Sarasamak K 2006 *Phys. Rev. Lett.* **97** 105502
[64] Zhang Y, Lu G H, Deng S H and Wang T M 2006 *Acta Phys. Sin.* **55** 2901
[65] Zhang Y, Lu G H, Hu X L, Wang T M, Kohyama M and Yamamoto R 2007 *J. Phys.: Condens. Matter* **19** 456225